2017

Visual Detection and Tracking Methods for *E. superba* (Antarctic Krill)

Regina R. Yopak
University of Rhode Island, yopak@uri.edu

VISUAL DETECTION AND TRACKING METHODS FOR *E.SUPERBA* (ANTARCTIC KRILL)

BY

REGINA R. YOPAK

A THESIS SUBMITTED IN PARTIAL FULFILLMENT OF THE

REQUIREMENTS FOR THE DEGREE OF

MASTER OF SCIENCE

IN

OCEAN ENGINEERING

UNIVERSITY OF RHODE ISLAND

2017

MASTER OF SCIENCE THESIS

OF

REGINA R. YOPAK

APPROVED:

Thesis Committee:

Major Professor Christopher Roman

Stephen Licht

Susanne Menden-Deuer

Nasser H. Zawia
DEAN OF THE GRADUATE SCHOOL

UNIVERSITY OF RHODE ISLAND

2017

ABSTRACT

Antarctic krill are a keystone species of the Southern Ocean. They have been well documented over large spatial scales but generally not quantfiably at the scale of single individuals in the open water column. It is important to study how individuals behave in their natural environment in order to further understand how they interact within dense krill aggregations. Using a pair of calibrated gray-scale stereo cameras mounted on a towed instrument sled, krill were imaged *in situ* at $10Hz$ in the bays along the western Antarctic Peninsula during austral winter 2013. Krill were identified and tracked through the images using a newly developed identification and tracking method that collates krill motion properties such as distance traveled, velocity and track duration using image processing techniques. Stereo geometry was used to define the krill motion data in the camera coordinate system and define the overall imaging volume to be approximately $2.0m^3$. The tracking method performed successfully for $60 - 80\%$ of tracks in a sample set of images. Difficulties in tracking krill successfully included excessive sled motion (heave), krill swarming (or schooling) behaviors and rapid changes in krill motion not accounted for by the tracking algorithm. An analysis of the krill velocities found that krill generally swam at less than $1m/s$ and increased to $2m/s$ while aggregating. This new imaging system successfully tracked and identifed krill in the midwater column and can be used to generate large motion data sets to better inform Antarctic krill behavioral and circulation studies.

ACKNOWLEDGMENTS

I would like to recognize my professor, Dr. Chris Roman, for his support during my graduate studies. I am also grateful for my lab mates (Clara Smart, Ian Vaughn, Gabrielle Inglis, and Dave Casagrande) for their constructive advice, humor, and never-ending encouragement throughout my graduate endeavors. To Dr. Susanne Menden-Deuer and Mary Kane who provided answers to all things krill-biology related, I am thankful for your thoughtful guidance.

Additionally I would like to thank my parents, Jessy, my aunt and uncle, Matthew, Jacob, and Mrs. A for their unending optimism, patience, love and countless dinners they provided which supplied me with all the energy I needed to succeed. And finally, to Paul: all my love and onwards!

PREFACE

Funding for this Masters degree was provided by a grant from the National Science Foundation (NSF) entitled *Collaborative Research: Seasonal Trophic Roles of Euphausia Superba (STRES) Grant*. The *STRES* grant supported two research cruises along the Western Antarctic Peninsula (WAP) during the austral winter (May - June) of 2013 and the austral summer (November - December) in 2014. This thesis was prepared in the manuscript format as described by the University of Rhode Island Graduate School.

TABLE OF CONTENTS

LIST OF TABLES

LIST OF FIGURES

Figure **Page**

MANUSCRIPT 1

Visual Detection and Tracking Methods for E.superba (Antarctic krill)

Regina Yopak [1];Mary K. Kane [2];Christopher Roman [3];Susanne Menden-Deuer [4]

is to be submitted for publication.

[1]MS Candidate, Department of Ocean Engineering, The University of Rhode Island, Narragansett, RI 02882. Email: yopak@uri.edu

[2]MS 2015 Oceanography, Graduate School of Oceanography, The University of Rhode Island, Narragansett, RI 02882. Email: cetaceansrule@gmail.com

[3]Assistant Professor (joint appointment), Department of Ocean Engineering/The Graduate School of Oceanography, The University of Rhode Island, Narragansett, RI 02882. Email: cnr@gso.uri.edu

[4]Associate Professor, The Graduate School of Oceanography, The University of Rhode Island, Narragansett, RI 02882. Email: smenden@gso.uri.edu

1.1 Introduction

Antarctic krill, *Euphausia superba*, play a prominent role in the Southern Ocean as the keystone species of the Antarctic ecosystem [2, 3, 4]. They are greatly affected by the most prominent factors of climate change which are ocean acidification and sea-ice retreat. Additionally, krill are major consumers of phytoplankton which are responsible for most of the carbon fixing in the upper ocean [5, 6]. Given these important roles it is necessary to understand krill behavior in order to further understand Southern Ocean ecology and implement better ecosystem management practices [2, 7, 5].

The bays along the western Antarctic Peninsula (WAP) (Figure A.1) provide a vital habitat in the krill life cycle, providing consistent shelter and phytoplankton food supply, making it one of the richest krill spawning regions in Antarctica [8]. Seasonal sea ice also protects krill larvae and juveniles by creating their overwintering habitat [9, 7, 8].

Krill distributions and abundances have been typically characterized over broad spatial areas using traditional methods such as ship-based acoustics and net tows, both of which tend to aggregate behavior [2]. Krill are infrequently studied at the scale of individual animals. Krill display significant spatial and temporal variability due to their life cycle migration patterns and swarming behaviors [3]. These behaviors impact other larger zooplankton species by providing or competing for food sources [10, 2]. In order to fully understand Antarctic krill ecology and how they impact their environment, small-scale behavioral data at the individual level needs to be further quantified and compared to larger scale observations [2, 4, 7].

Imaging systems are potentially useful tools to study small zooplankton, such as individual krill *in situ*, and yield accurate behavioral motion data and abun-

dance estimates [11, 12, 13, 14]. Midwater camera systems have been used in limited fashion to image krill populations. When used, imaging systems are often mounted on net tows to ground-truth observations or deployed independently to identify taxa in the water column. Cameras, such as the Video Plankton Recorder (VPR), have been used in conjunction with a Multiple Open and Closing Net with Environmental Sampling System (MOCNESS) to estimate krill abundances (or other zookplankton) using the paired net and image data [13, 15, 9, 16, 17]. Studying krill (and other zooplankton) behavior using a net-mounted camera is also limited by the documented net avoidance behavior of euphausiids [9, 18].

In an effort to further methodologies for studying zooplankton behavior *in situ*, this paper describes the detection, identification and quantification of krill motion in the water column using image data from a midwater camera system. *In situ* imaging can offer behavioral and three dimensional motion data that traditional sampling methods cannot, while providing insight into the validity of laboratory-based experiments. To detect and track krill through collected images, a general method was devised to identify krill based on their shape and aspect ratio, and then track individual animals through image sequences. With this approach krill were succesfully identified and tracked forward and backward in time to create a database of motion tracks and associated data such as speed, aspect ratio and size.

Image data were collected using a stereo camera sled during the May - June 2013 *Seasonal Trophic Roles of Euphausia superba (STRES)* research cruise aboard the *RVIB Nathaniel B. Palmer* in the bays along the WAP. The camera sled was deployed 40 times at the locations highlighted in Figure 1. Additional MOCNESS data were collected and analyzed during this cruise to identify zooplankton taxa and abundances at the dive sites [19]. Initial krill distributions using image data from the camera sled were examined as well [11]. The austral winter season pro-

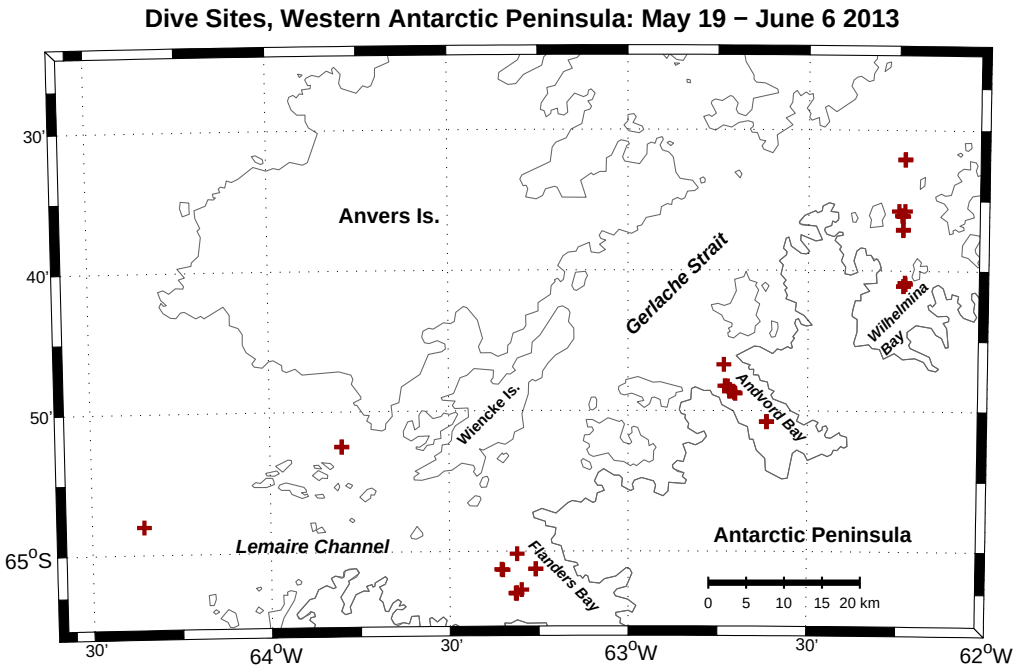

Figure 1: Camera sled deployment sites. The majority of deployments took place in Flanders Bay, Andvord Bay and Wilhelmina Bay.

vided a low turbidity water column to image the krill [9, 3, 20, 4]. In general, only *E.superba* were collected in the net tows and observed by the cameras.

1.2 Materials and Methods

1.2.1 Camera Sled and Image Data Acquisition

The camera sled system (Figure 2) was designed and built for the purpose of imaging biota ($1cm$ - $6cm$ in length) in the water column. The sled is rated to $2000m$ water depth and offers the ability to observe the water column in real time on the ship. The sled system contains a stereo pair camera, Sea-Bird 49 FastCAT CTD, a $1200kHz$ ADCP, a lightfield camera and LED lights (red and white) to illuminate the field of view (Figure 2a) [21, 9, 17].

The sled can be used to image in side-looking or down-looking orientations

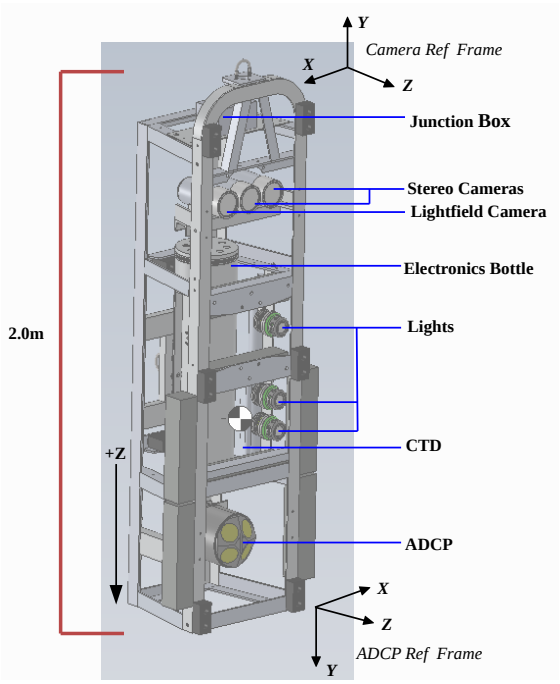

(a) Camera sled specifications.

(b) Side-looking configuration on deck.

Figure 2: The camera sled. (a) The system is approximately $2.0m$ in length and has a gray-scale stereo camera pair, lightfield camera, conductivity, temperature and depth (CTD) sensor and a $1200kHz$ acoustic doppler current profiler (ADCP). The mounted LED lights illuminate the camera field of view. The electronics bottle houses the power electronics and communications interface. (b) The camera sled is prepared for a dive in it's side-looking position.

while profiling different depths or being towed through the water (Figure 3). For this paper only the side-looking images are used (Figure 2b). Two Manta G-145B NIR cameras with Fuji HF9HA-1B lenses are mounted in $2000m$ flat port pressure housings. The 1038x1388 8-bit grayscale images are collected at $10Hz$. Typical dive depths ranged from $250 - 1500m$, with images collected from the surface to within two meters above the bottom. The camera's field of view was calibrated and focused (Figure 4) to image approximately $1.8m^3$ [10, 12]. The in-focus, sample volume was chosen to prioritize a larger depth of field at the expense of some resolution to track krill rather than perform species identification.

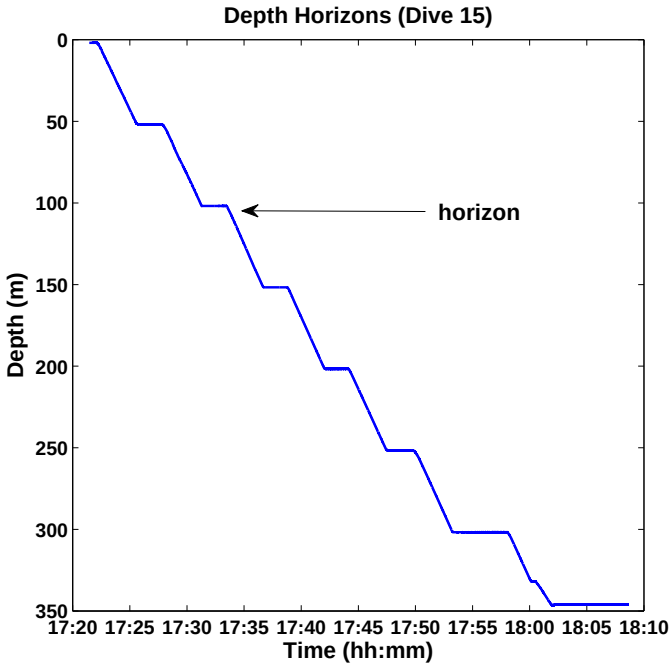

Figure 3: In this example the camera sled descends and stops every 50m at depth horizons in the water column for about 2 minutes each to collect image data.

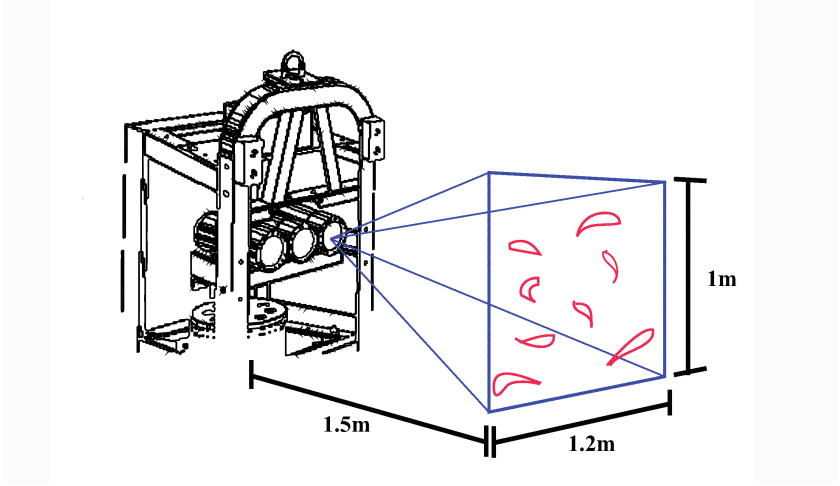

Figure 4: Each camera has an approximate 1.0m tall by 1.2m wide field of view in focus to approximately 1.5m from the camera.

1.2.2 Krill Identification

Krill were identified in each image using the following series of processing techniques implemented in MATLAB®.

Figure 5: An initial gray-scale krill image from the stereo pair which has been initially filtered with a high-pass filter to increase edge contrast around the krill and remove any light patterns.

1. The initial gray-scale images (Figure 5) are high-pass filtered to remove the background illumination pattern in the image and better define contrasting edges (Figure 6a) [22, 23].

2. Each gray-scale image is thresholded to produce a binary image (Figure 6b). A threshold value for each image is determined in MATLAB® using Otsu's method and averaged over a window of every 10 adjacent images [24].

3. An elliptical structuring element (SE) of radius five (Figure C.1) is used to morphologically open the binary images to identify possible "krill" [22, 23].

4. Each pixel cluster after the opening operation is considered a possible krill. The identifying properties (area, major and minor axes lengths, and centroid position in pixels) are catalogued.

5. The aspect ratio and pixel area are used to reject potential false krill identi-

(a) Initial gray-scale high-pass filtered krill image.

(b) Converted to binary krill image.

(c) Morphologically opened krill image.

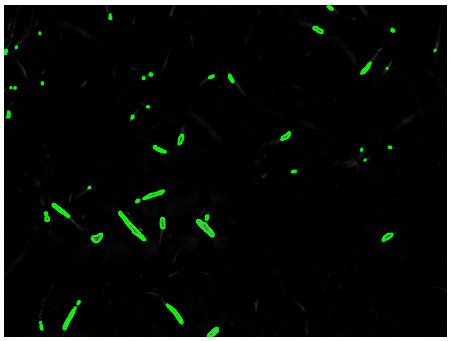

(d) Possible krill identified and bounded in the original image (a).

Figure 6: An example of the image processing that identifies possible krill (a-c). The filtered krill are highlighted in (d).

fications. The aspect ratio for a krill should be greater than three. The krill size should be greater than 400 pixels (Figure 6c) [11].

6. Each positively identified "krill" in an image is indexed and an initial krill count per image is produced. The accepted krill are highlighted in green over the original gray-scale image (Figure 6d).

An elliptical shape was chosen to open the binary image due to a krill's generally tapered elliptical (two-dimensional) shape [22, 21, 25, 23]. To verify that the segmentation algorithm was successfully identifying krill, a comparison between a traditional human krill count and the automated count was completed. One hundred random images containing krill from the same dive were chosen and manually

counted. The algorithm was then run with two differently sized structuring elements to identify krill. The two automated datasets and the human visual count are compared in Figure 7 with a linear regression describing the agreement between the algorithmic and traditional counts.

Figure 7b demonstrates that the stricter (larger) structuring element size helped the algorithm correctly identify more krill than the small structuring element. The small structuring element was prone to identifying more small zooplankton or detritus as possible krill than the larger element (Figure 7a). This demonstrates that the algorithm satisfactorily segments krill from the images using the larger structuring element.

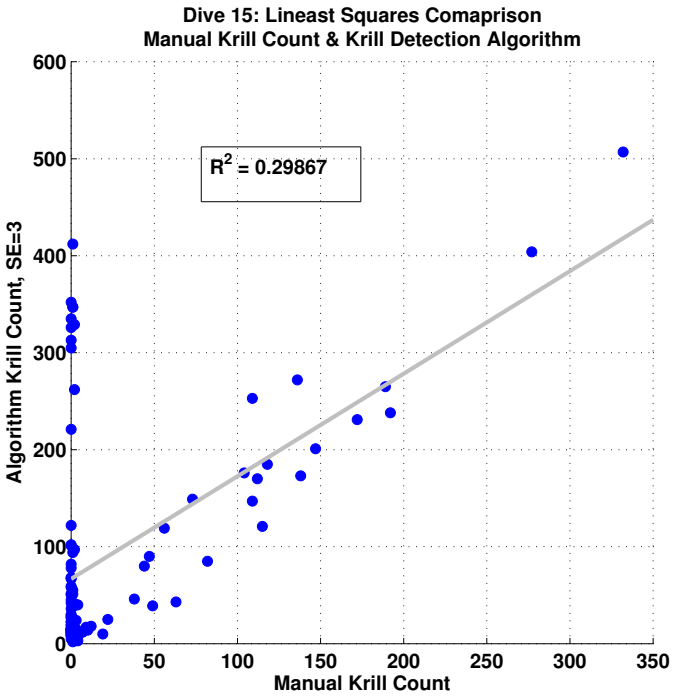

(a) Structuring element (SE) with radius of 3.

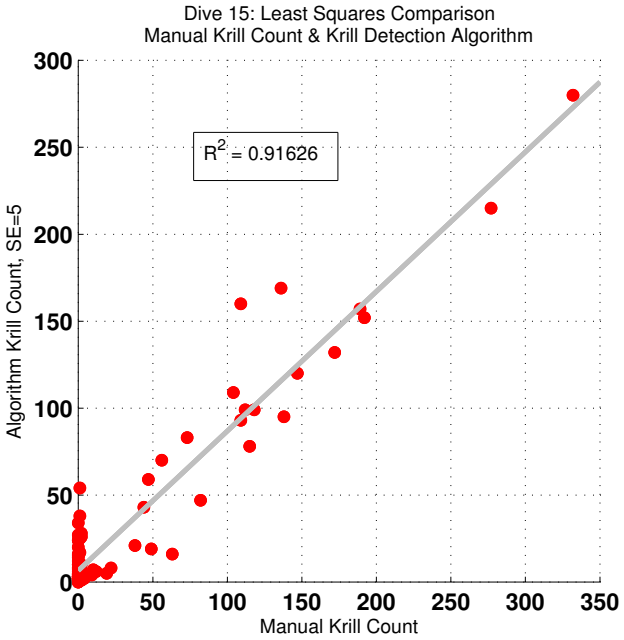

(b) Structuring element (SE) with radius of 5.

Figure 7: The automated krill identification and a traditional visual krill count per image are compared for 100 images using a linear regression. The structuring element with a radius of five performed better for krill identification.

1.2.3 Krill Tracking

Using krill properties provided by the identification step, krill can be tracked between image frames. The general automated krill tracking method is described below.

1. An initial krill to track is chosen from the image data from the initial segmentation algorithm with the constraints that it has an aspect ratio greater than three and a size greater than 400 pixels [11]. All krill selected satisfy these requirements.

2. This krill is given an identifying *global krill number* to flag it through the adjacent images forward and backward in time.

3. In the image sequence, possible matches are searched for within a set radius ($100 pixels$) from the krill's position in the prior image. Krill, on average, did not travel more than 100 pixels between image frames when swimming in a steady manner.

4. For all possible matches motion vectors relative to the initial krill positions are calculated. These vectors are compared to an estimate of the krill's prior motion, if available. A trajectory angle for each possible match is calculated and used to calculate the vector dot product to help relate possible matches [26]. If this is the first krill in a track, a motion vector cannot be calculated but a vector dot product is for all possible matches to help relate them to the initial krill.

5. If a prior track exists, a predicted position in the adjacent image can be calculated and used to evaluate possible matches. A match is selected if it is closest to the predicted position out of the pool of possible matches. If no

prior track exists, a match is chosen based on the distance and how similar the initial krill's pixel properties (area, aspect ratio) are to possible matches.

6. To check if a match has been made correctly, and a prior track exists, the match's krill properties have to be within one standard deviation of each of the initial krill's along-track collated properties (velocity, aspect ratio, angle and distance traveled) satisfying the criteria in Figure D.1. If no prior track exists to check against, then the match's properties are compared to the initial krill's properties using area and aspect ratio. They must be less than or equal to the initial values in order to be a good match.

7. If the above conditions are met for a krill, the selected match is kept. The matching krill's newly calculated properties (aspect ratio, position, dot product, angle, velocity etc.) are recorded to be used in the next tracking iteration.

8. If a match is not made, the search radius is expanded to $200 pixels$ and the tracking method attempts to make a new match a second time. If it fails to match the second time, the track is ended.

Tracking continues through sequential images for the selected krill by it's *global krill number* until a match cannot be found. This may be because the krill has left the image frame or no potential krill are within the search radius. The properties associated for every image the krill is tracked through (distance traveled, aspect ratio, velocity and angle) are recorded. Figure 8 plots an sample krill track made up of 20 images ($\sim$ 2 seconds).

The tracking method can be run forward or backward in time as long as the images are sequential. Krill tracks can be started using krill that follow the relatively strict criteria of a radius of five and an area equal to or greater than

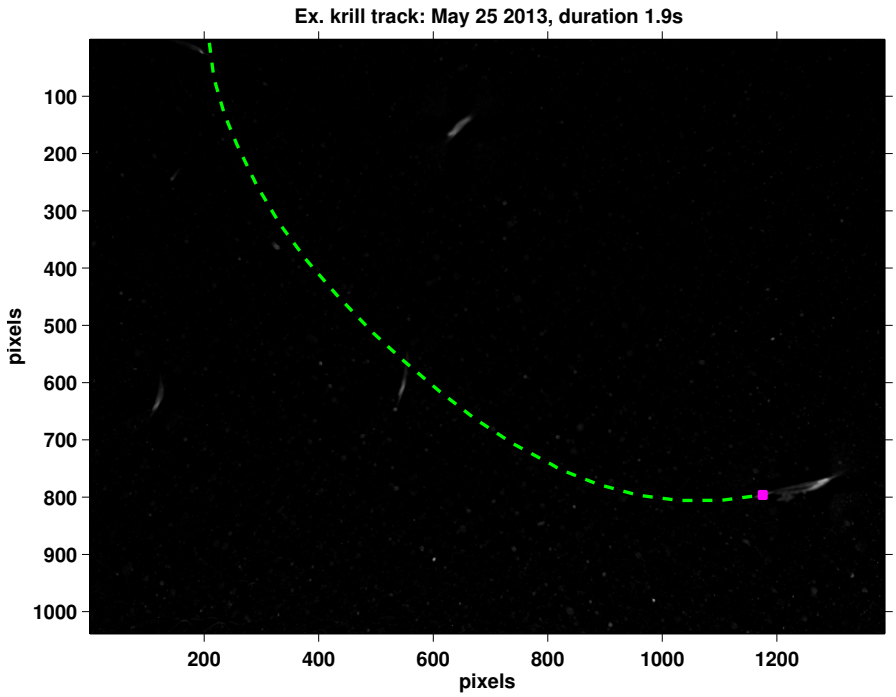

Figure 8: A krill tracked through a sequence of 20 images.

$400 pixels$ (Figure 7a). This ensures tracks are started on actual krill and not falsely identified particles. Once a track has been started the possible matches can come from a less strict pool of candidates that satisfies the criteria of a radius of three and no pixel area limits. This allows tracks to include identified krill that may not have been considered confident enough to start a track. This less restrictive identification method generates more potential matches and longer tracks but also does not necessarily only identify krill in the image [22, 27, 23]. Krill that are matched to a track cannot be matched again. To increase efficiency, the automated tracking method retains the calculated properties of the krill to avoid recalculations [23, 27].

1.2.4 Synthesis of Krill Motion Data

An organizational structure for the krill motion data is created after tracking krill through an image directory. The tracking method produces three data

Dive 23, Horizon #8: Recorded Krill Track Properties for Image 88

Global #	Pixel Velocity ($pixels/sec$)	Position (xy)	Aspect Ratio	Trajectory, θ (rad)
414	426.1	[113 841]	2.6	0.0511
415	426.1	[177 841]	1.7	0.0120
416	279.1	[396 836]	2.2	0.0266

Table 1: Table of three individually tracked krill (identified by their *global krill number*) recorded in a single image.

structures, each indexed by image number and *global krill number*. The following bullets describe each data structure.

1. A *properties array* stores all krill data (position in the image, aspect ratio, area (in $pixels$), velocity (in $pixels/sec$), distance traveled (in $pixels$) and trajectory angle (θ)).

2. A *tracks array* flags (using binary identifiers) when a krill is present in an image or not.

3. An *image list* is a list of image names used by the krill tracking algorithm.

An image directory can be visualized (Figure 9) and individual track data can be referenced by image number and *global krill number* (Table 1). Other examples of the track catalogue functionality includes viewing all krill tracked in any given image (Figure 10a), and viewing a single track or multiple tracks present in an image set for a period of time (Figure 10b).

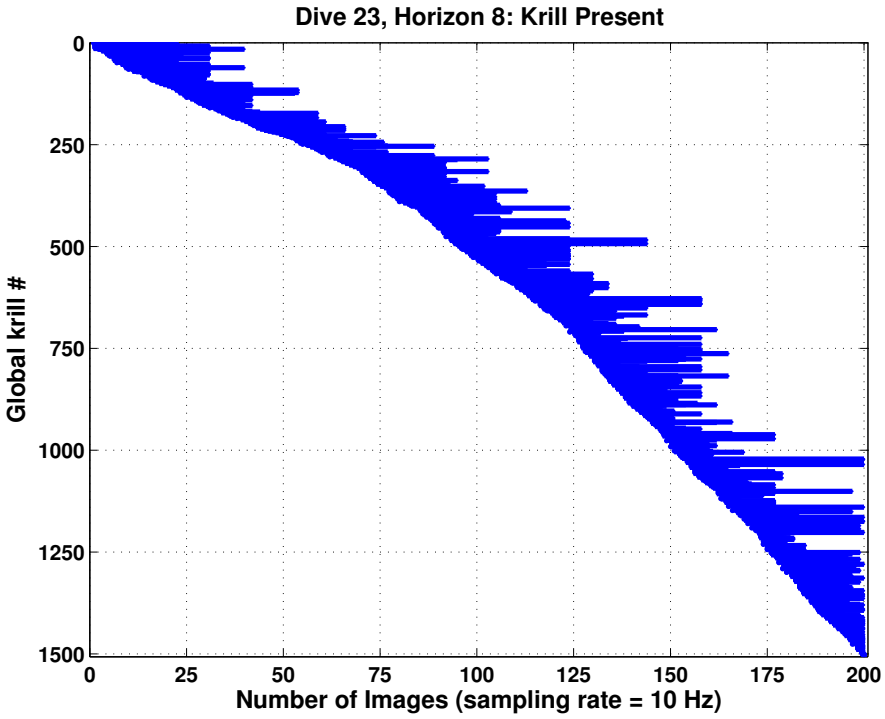

Figure 9: A graphical sample of 1500 krill track lengths by global indexing and image number.

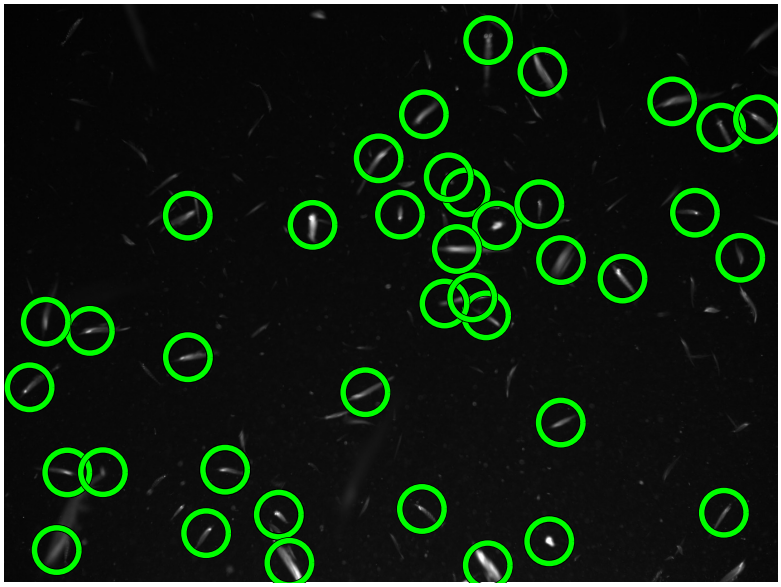

(a) Identified krill.

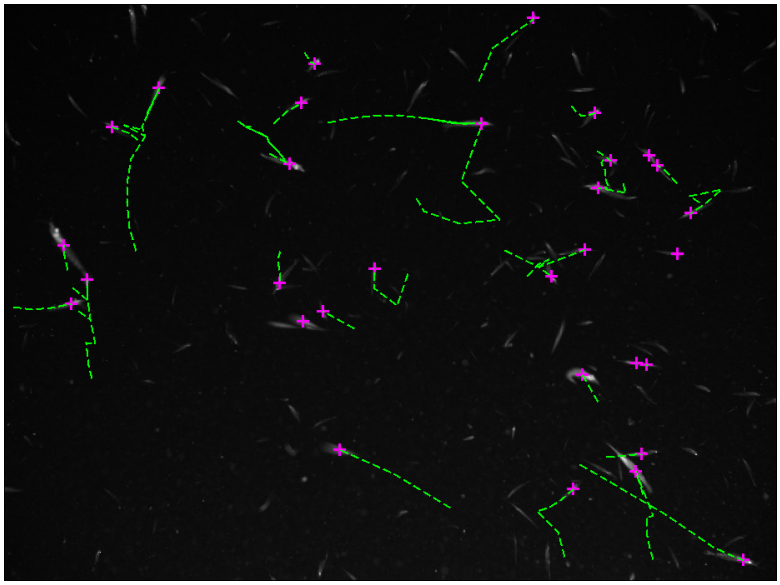

(b) Krill tracks.

Figure 10: Krill motion data is from dive 23 on May 29, 2013 in Flanders Bay, Antarctica. (a) All tracked krill are identified in one image frame. (b) Tracked krill in a single image are shown with their prior tracks from previous images.

1.2.5 Krill Camera Geometry: Relative Velocities

In order to analyze krill motion data in a euclidean reference frame, rather than in pixel coordinates, the data are transformed using the stereo camera geometry and triangulation methods detailed in [1, 23, 28]. To generate the stereo information a tracked krill in the left camera must be correctly matched in the right camera image.

This correspondence problem is solved by rectifying the stereo images following procedures described in [23]. The intrinsic and extrinsic properties of each camera are known through a calibration done prior to fieldwork [29]. An image rectification transform to the left and right images makes them co-planar (or rather, horizontally collinear) to one another. Once the images are co-planar, the epipoles in each are sent to infinity (Appendix B.1) making the epipolar lines collinear to one another.

Once rectified, matching krill between image pairs becomes a 1-D search across the adjacent image rows [1, 23, 26]. A normalized sum of squared differences (SSD) is used to match krill between corresponding left and right images. Images are normalized (I_{norm}) before performing the SSD by

$$I_{norm}(x, y) = \frac{I - \overline{I}}{\sqrt{\sum \left(I - \overline{I}\right)^2}} \tag{1}$$

where $\overline{I}$ is the average image intensity. The SSD is calculated as,

$$SSD = \sum_{u=-W}^{W} \sum_{v=-H}^{H} [I_R(x + u, y + v) - T(u, v)]^2 \tag{2}$$

where a square 40x40 pixel template (T) is created centered on a krill's position in the left image (I_L), and a 1-D epipolar search (along the adjacent image rows) is performed across the normalized right image (I_R) for a match. This ensures the template and image are comparing the true variance in intensity values. In this case the SSD values range between zero and one, and the minimum SSD value denotes the matching position (Figure 11). The stereo krill matching is run as a

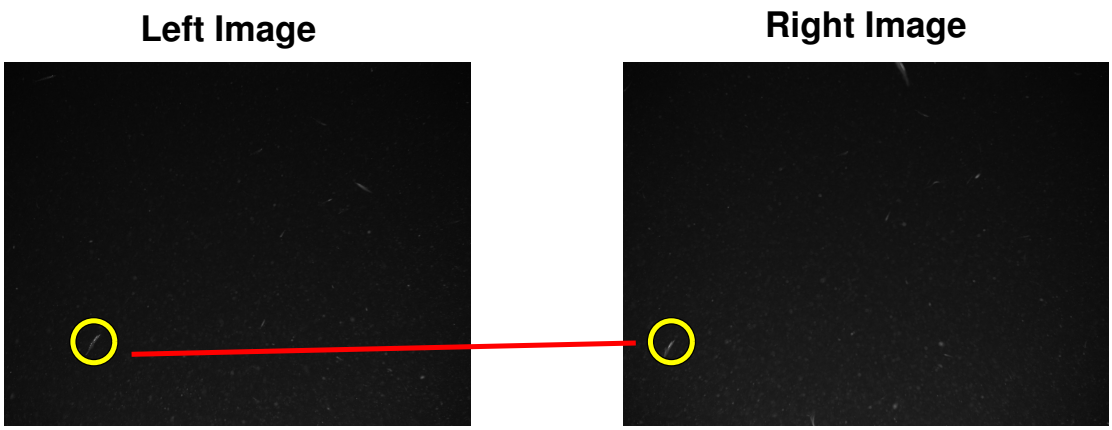

(a) Matched krill (global number = 28) between respective left and right images.

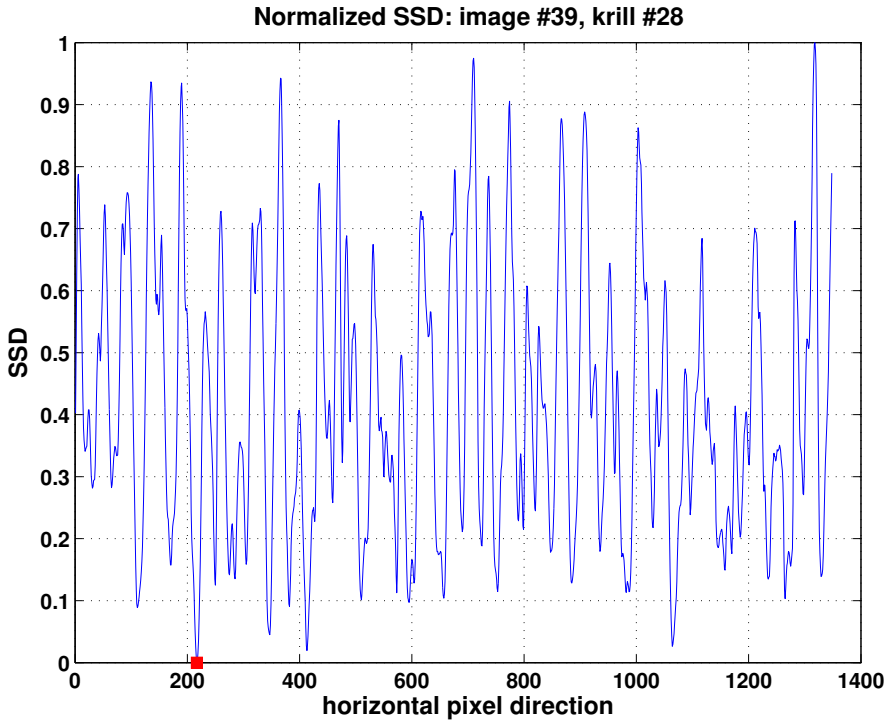

(b) Krill Number = 28 (yellow circles), image 39.

Figure 11: (a) A krill is matched between rectified images. (b) A SSD is used to find a matching krill between images.

batch process for all tracked krill and matched krill and have their camera relative positions (uv in *pixels*) appended to the track library. These matches are then triangulated using a stereo reconstruction technique to calculate three dimensional positions in the camera coordinate frame [1]. Table 2 lists the krill track statistics

appended to the track library data structures that are now reported as distance traveled (m), instantaneous velocity (m/s), and velocity components (V_{xyz} in m/s).

Camera Depth of Field

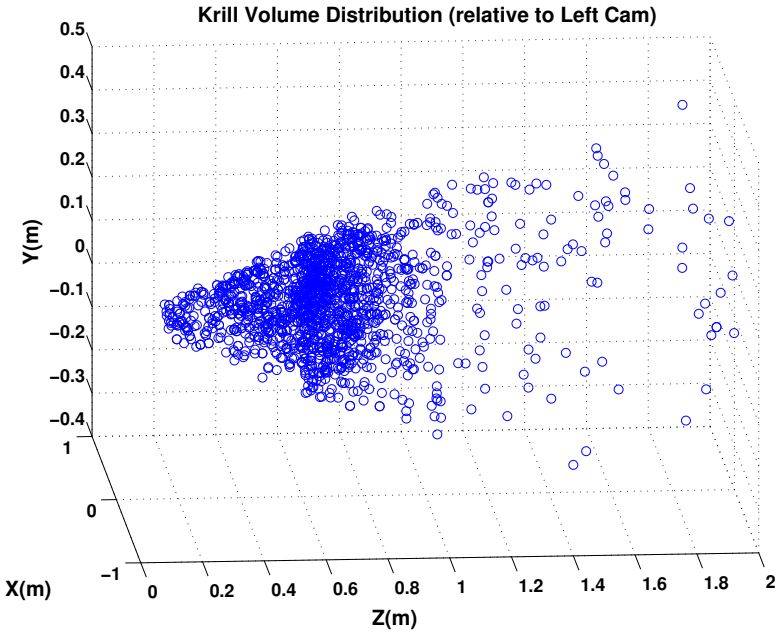

Figure 12: A random set of triangulated krill positions from 1000 images plotted in the camera reference frame. This shows the effective imaging volume of the camera system.

The stereo transformation of individual krill provides a direct description of the imaging sample volume. A random set of 1000 images was chosen from the same dive, and each krill identified by segmentation was stereo matched and triangulated. The resulting 3-D positions (Figure 12) show that the majority of identified krill were $0.6m$ to $1.0m$ from the left camera. The minimum and maximum distances were approximately $0.2m$ and $2m$ respectively. The cameras had an estimated depth of field of $1.8m$ and a sample volume of approximately $2m^3$.

Water Relative Velocities

Krill velocities are computed using their distance traveled (in meters) from stereo triangulation and track duration (in seconds). Calculated velocities are relative to the camera, and not the surrounding water (uncorrected V_{ave}, Table 2). To determine water relative krill motion, water velocities measured with the ADCP were compared to the krill velocities at the same time (Figure 13). The calculated krill motion data and ADCP water velocity data from the first range bin ($2.5m$) are matched using time stamps and then oriented using the instrument's coordinate frame (Figure 2a). In general the magnitude of ADCP water velocities are small ($0.2m/s$), relative to the observed krill velocities (Figure 13). Along track velocities can be corrected to produce water relative measurements using the ADCP water velocity data. This is discussed in section 1.3 where resulting krill position and velocity trends are examined.

Krill Track Statistics

krill number	track duration (sec)	distance (m)	uncorrected V_{ave} (m/s)	corrected V_{ave} (m/s)
23	3.1	0.351	3.96	3.94
127	2.2	1.37	2.52	2.50

Table 2: Two examples of the differences in krill motion (for two unique krill) relative to the camera sled versus relative to the water.

Krill velocities and tracks can be shown in both two dimensions and three dimensions (Figure 14). The three dimensional tracks (Figure 14b) also highlight the variability in krill positions in the z direction which is most likely due to triangulation error [1, 23, 28].

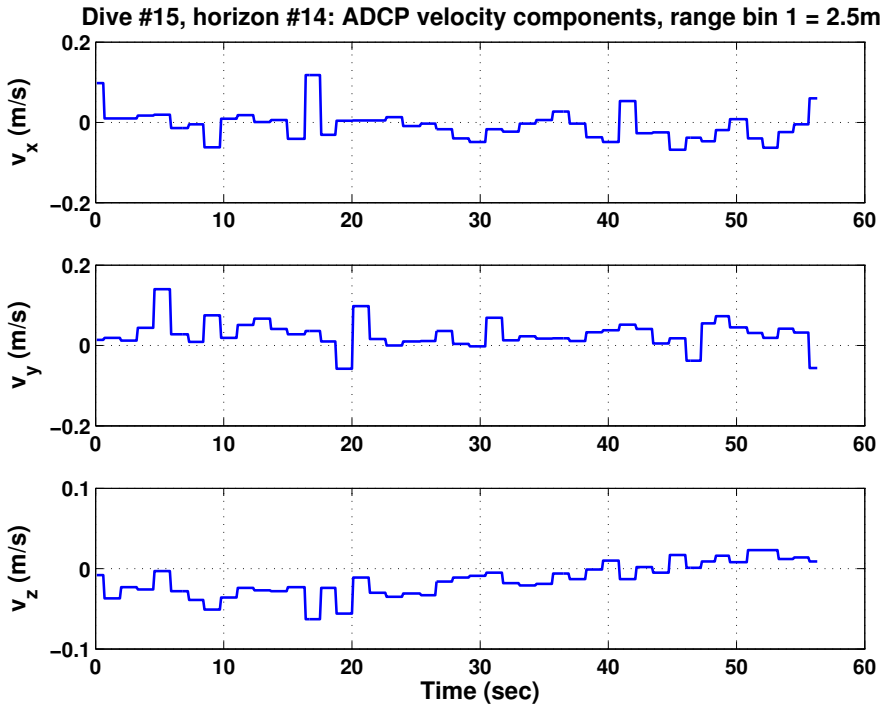

Figure 13: Sample ADCP velocity components over one minute show the water motion relative to the cameras. The water velocities are generally small relative to the krill swimming velocities.

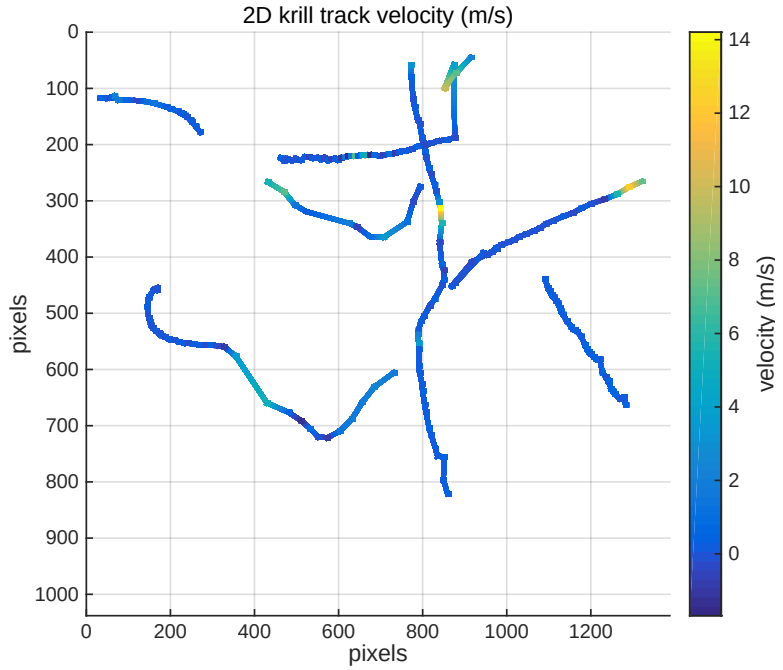

(a)

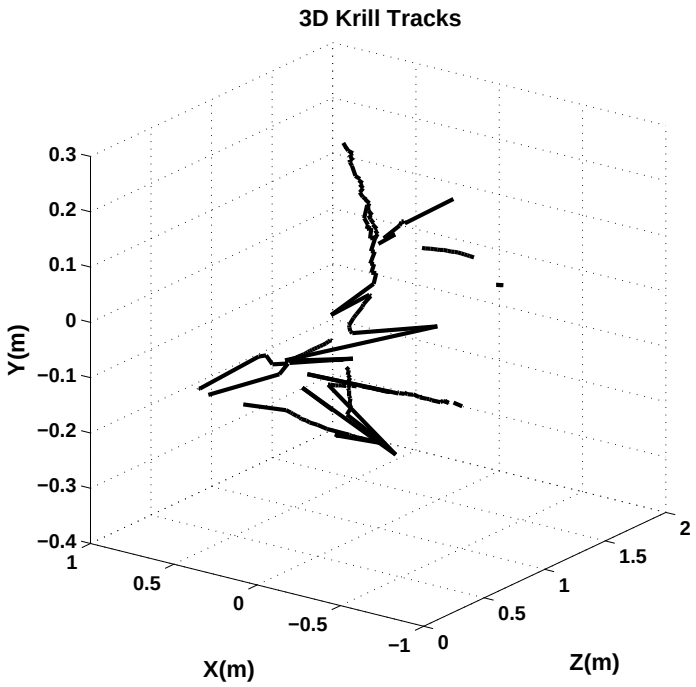

(b)

Figure 14: Six example krill motion tracks. (a) Two dimensional track paths in pixel coordinates are overlaid with calculated velocities. (b) The same tracks are plotted in three dimensions in camera relative coordinates.

1.3 Results

To test the performance of the tracking algorithm four dives were analyzed. This includes 17 depth horizons encompassing daytime and nighttime periods. Approximately 4000 krill were tracked. In general, tracking worked best for images with less than 20 krill. Common problems were bad tracks caused by high krill population images such as krill swarms, rapid accelerations or krill leaving the field of view. High population krill images contain large amounts of motion and too many possible matches which made it difficult to track individual krill successfully. These images generally had shorter tracks or bad tracks (ie. false tracks that are populated by bad matches), and contributed to the outliers in the track statistics. This trend is demonstrated in the overall dive statistics with an average track length of $0.05m$, velocity of $3.71m/s$ and a duration of $4.05sec$ (Table 3).

Basic Track Statistics

Track	ave	max	min
length(m)	0.05	0.55m	0m
velocity(m/s)	3.71	14.0	0.03
duration(s)	4.05	13.7	0.10

Table 3: Basic krill track statistics from four dives (14, 15, 16 and 23).

1.3.1 Automated Tracking Performance

To assess the errors in more detail dive 15 was chosen to estimate what percentage of tracks are successful versus incomplete for a set of images. This dive was chosen since it has the greatest number of uncorrupted depth horizons, meaning ship heave or pervasive krill swarms did not dominate the majority of image data, out of the entire dataset. An incomplete, or bad, track is defined as a continuous motion trajectory that has been split into two or more tracks, or a track populated by bad matches (Figure 15). This means they are identified in the track data library with multiple *global krill numbers* resulting in over counting and er-

roneously short tracks. A good track is defined as a continuous motion trajectory that starts with the krill appearing in an image and ending when it leaves the frame or becomes too small to track.

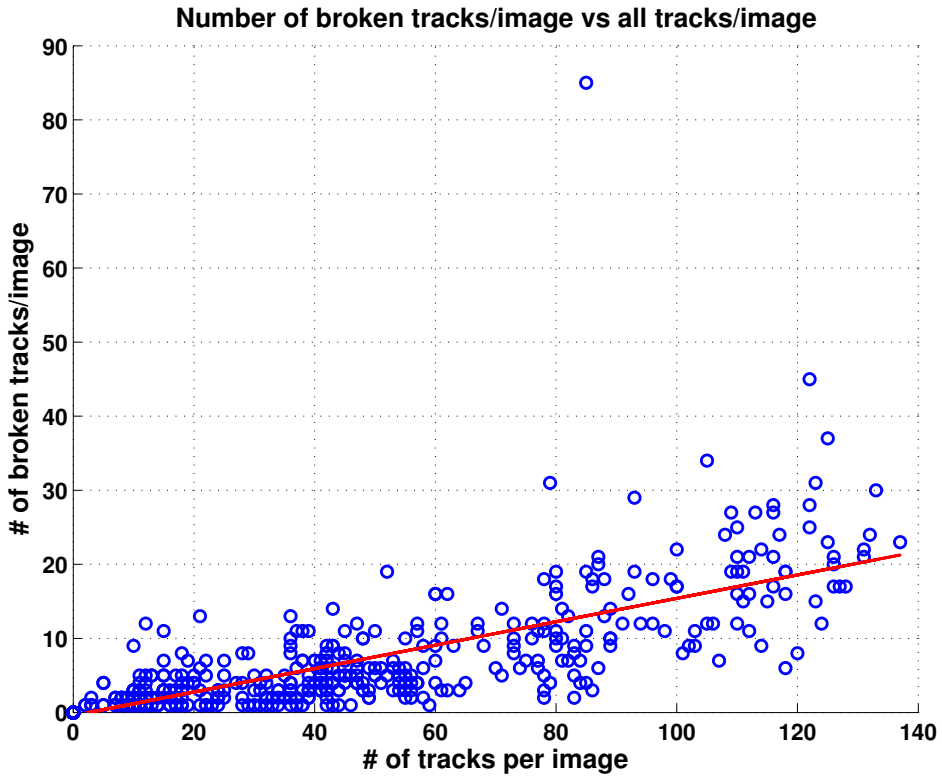

Figure 15: Demonstrates that as the number of tracks in the image increase so does the number of possible broken tracks. Broken tracks are identified by the automated tracking method.

In high population krill images ($> 15 - 20$ krill), where there are many tracks occurring, incorrect matches in sequential images happen due to the large number of possible krill to associate with a given track. This corrupts the track by switching to a new krill mid-track. Rapid accelerations between image frames also causes tracks to end prematurely. These accelerations move the krill outside of the match search radius, which causes the track to end or make an incorrect match with a krill inside the search radius. The search radius was adjusted to account for rapid motions on average, but since the movement in pixels is a function of range a single

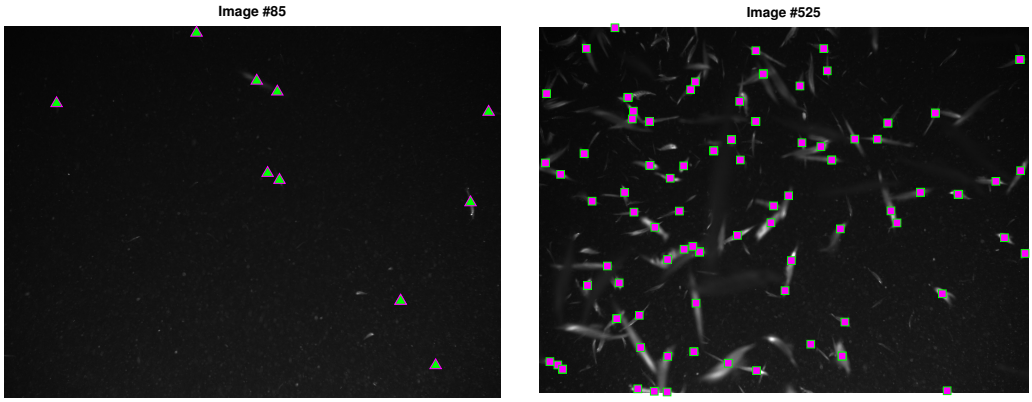

(a) (b)

Figure 16: The tracking method performs better for (a) low krill population images than for (b) high population images.

Tracking Performance

	Manual	Automated
good	63%	79%
bad	38%	21%

(a)

Manual

corrupt	broken	
21%	17%	
	not fixed 8%	likely fixable 9%

(b)

Automated

corrupt	broken	
3%	18%	
	not fixed 16%	fixed 2%

(c)

Table 4: Data from 100 random tracks, from Dive 15/horizon #14, are compared. (a) The number of good and bad tracks for the automated versus manual checking. The manually checked identified percentage of good tracks is more conservative (63%) than the automated checking percentage (79%). (b & c) The bad tracks are separated into two types of incomplete: corrupted and broken.

radius will not solve the entire issue.

A random set of 100 tracks (a mix of high and low krill populations) (Figure 16) were selected and checked for the number of good and bad tracks manually and with an automated check (Table 4a). The automated track check goes through the track data and flags potentially broken tracks and attempts to fix then based on how close in image position the broken tracks are and if the break occurred

over sequential images. The automated checking identified a higher percentage of good tracks ($\sim$ 79%) while the manual identification produced a more conservative estimate of good tracks ($\sim$ 63%). To determine whether any of the bad tracks could be fixed they were split into two categories: corrupted and broken (Table 4b and 4c).

"Corrupted" meant the track wasn't capable of following the animal and "broken" means a fix was attempted as part of the automated track check. Tracks can be fixed if a track's ending location in the image is within 100 pixels of a new track's starting location in the adjacent images and the new krill has a similar aspect ratio. Such tracks are rejoined and the *global krill numbers* are shifted to account for the fix. If the break is not within 100 pixels of a new start the broken track is not fixed (Table 4b and 4c). For the random track set a larger percentage of broken tracks (38%) were identified manually than with automated checking (21%). The percentage of broken tracks that could be fixed manually or automatically is comparatively similar at 9% and 2%, respectively (Table 4b and 4c).

In total this sample suggests that 60% to 80% of tracks (Figure 17 and Table 4a) are successful (or complete) for a given image set. This estimate can be applied to a general track count per image (Figure 17).

1.3.2 Tracking Compared to Identification Performance

There are several differences between the initial segmentation techniques to identify krill in an image and the automated krill tracking that associates potential krill with motion tracks. Segmentation uses only information in a single image to identify possible krill. This requires that the criteria to determine a krill needs to be restrictive enough to avoid false positives. The automated tracking process uses a two-step krill identification. First, krill are selected to start a track based on the

same criteria as the initial krill identification method, using the more restrictive (large radius, $r = 5$) morphological operator and set pixel area (> 400). Second, subsequent krill are identified and added to the track using a less restrictive (small radius, $r = 3$) morphological operator and prior track characteristics (position, speed, trajectory angle etc.). This produces a larger pool of possible matches in each image, and includes animals that would have originally been discarded for fear of false positives. This allows more krill to be identified in the subsequent images, leading to more krill successfully identified per image using the automated tracking rather than the single image segmentation method alone (Figures 17 and 18).

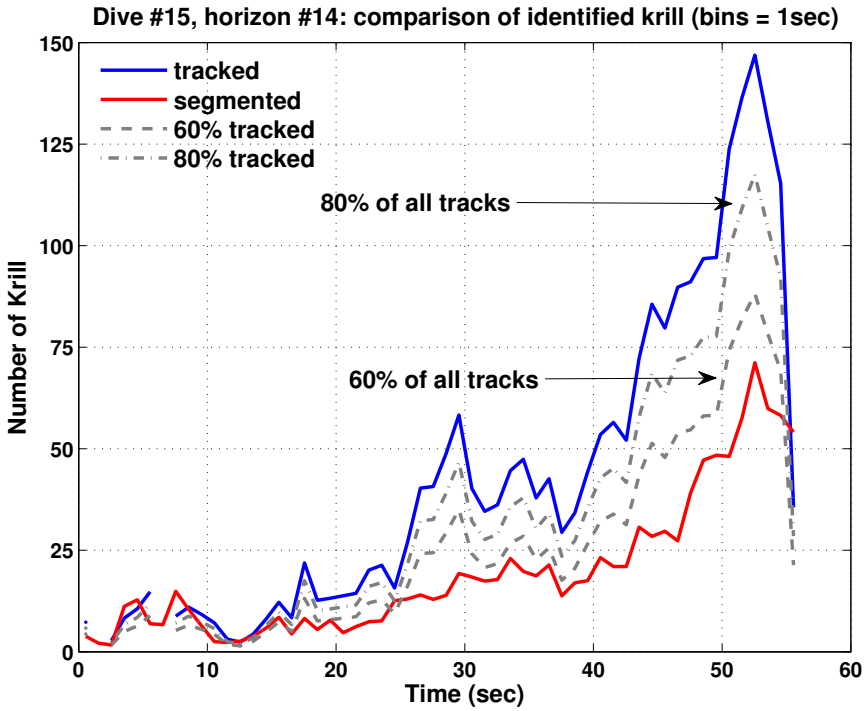

Figure 17: A higher number of krill are tracked using the tracking method than the segmentation only techniques even when considering only $60 - 80\%$ of tracks are good and unbroken.

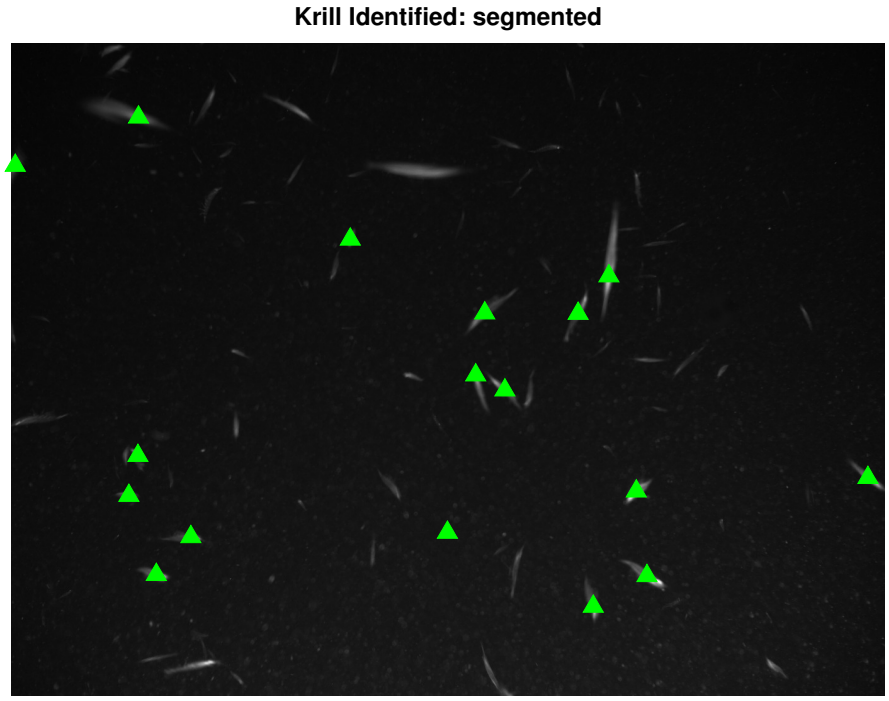

(a)

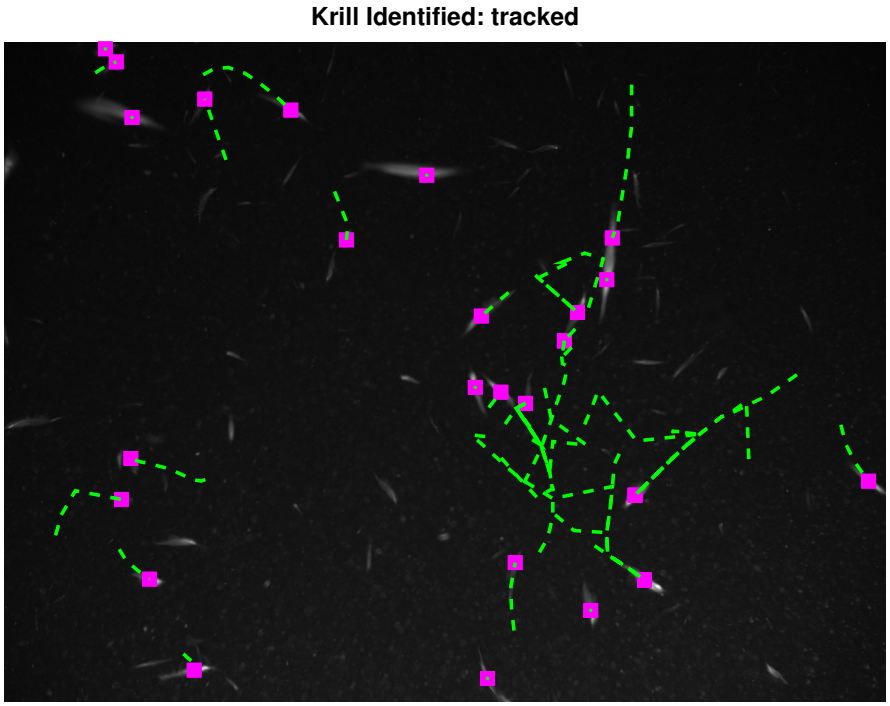

(b)

Figure 18: Krill identified from the track library and segmentation only method. Fewer krill are identified using the segementation techniques than using the automated tracking algorithm. In this sample image segmentation identified 17 krill (a) while the automated tracked identified 25 krill (b). (Note: some krill locations overlap due to proximity).

To compare the number of krill identified using the automated tracking algorithm in comparison to the initial segmentation techniques depth horizon #14 from dive 15 was used. Krill counts from tracking and segmentation were compared and it was found that the automated krill tracking identifies more krill than using segmentation alone (Figure 17). The number of good tracks per image were estimated using the successful track estimate (60% - 80%) from the earlier tracking performance assessment (Table 4). This result can also be seen in example images showing the krill identified with the segmentation and tracking methods (Figure 18).

1.3.3 Krill Position and Velocity Trends

The stereo camera geometry is able to derive krill positions in 3D and the associated velocities (Figure 14). The resulting position data has noticeable variability along the z-axis (Figure 14b).

By plotting a random set of 20 velocity tracks and subtracting the average velocity for each direction (Figure 19), it is clear that V_z has the greatest variability. ADCP water velocties were plotted for the same depth horizon to determine how much the observed water velocties were contributing to krill motion (Figure 13). The ADCP velocties were found to be small suggesting that water velocities are not significantly contributing to krill motion variability (Figure 19).

This velocity variability in the z-direction is most likely due to the error associated with triangulating positions during the stereo reconstruction. Triangulation in pixel location has the weakest constraint in z (Figure 19) and is easily effected by small errors when matching krill centroids between images [23, 1, 28].

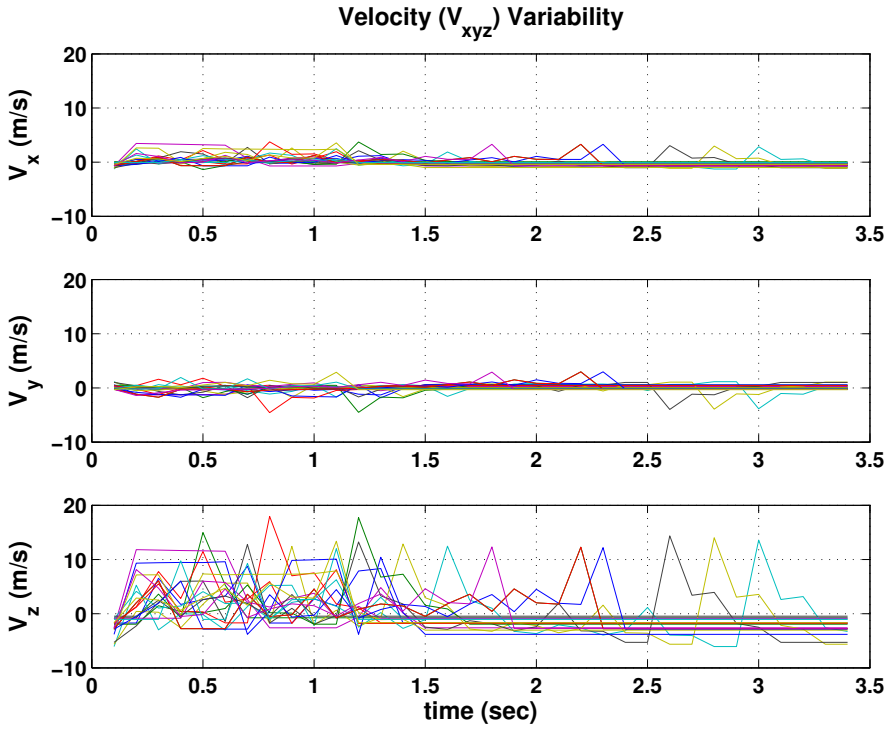

Figure 19: Detrended velocity components (the mean is subtracted for each) for 20 krill tracks. The z-direction that has the greatest variability and the dominant direction of calculated krill motion.

1.3.4 Velocity Distributions

Krill velocities over an entire dive show the distribution and range of observed velocities. Dive 15 is used since it has the highest number of depth horizons and associated track data for generating ensemble statistics. The majority of krill velocities observed were under $5m/s$ (Figure 20a) and an overall average velocity of $2.15m/s$ was observed.

The whole dive is broken down into individual horizons and displayed with population statistics. It shows that all horizons have medians and set average velocities of less than $2.5m/s$. It is highly unlikely those high, outlier velocities are accurately tracking krill (red points in Figure 20b) considering observed krill velocities in lab based experiments have shown that krill generally swim at speeds of less than $1m/s$ [10].

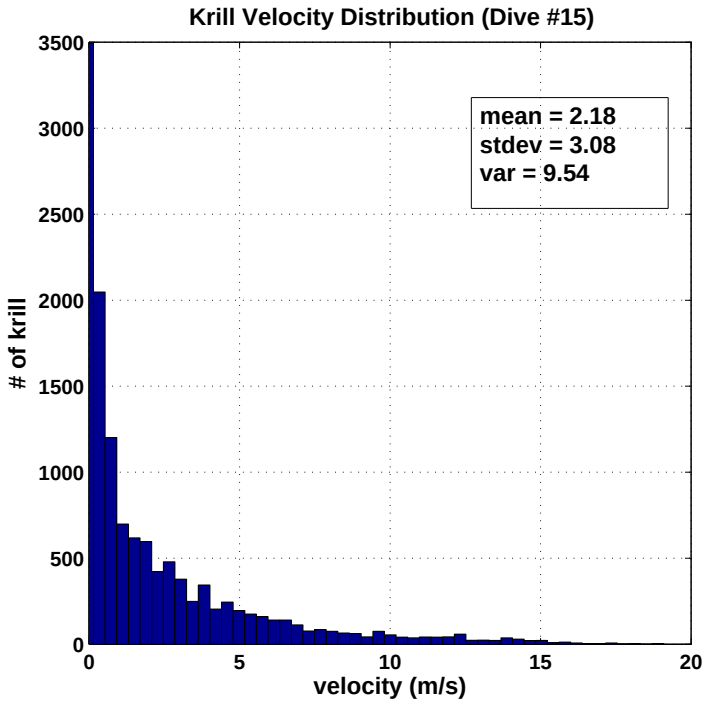

(a)

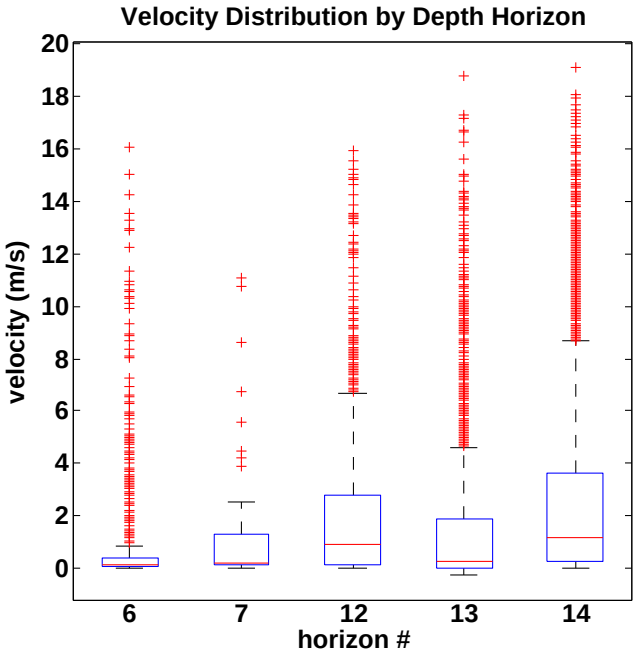

(b)

Figure 20: The krill velocity distributions for dive 15. (a) Histogram of observed velocities split up by horizons. (b) Velocity with set distributions statistics for each. There are many outlier velocities which do not fall into the box plot quartiles and greatly influence the velocity trends overall.

However, sustained velocities upwards of $2m/s$ have been observed in the open water column [30, 31]. Therefore it is unlikely that any velocities over $2m/s$ are accurately reporting krill motion and that the high percentage of velocity outliers (Table 5) are forcing the median and average krill velocity values higher than they actually are. The horizon velocity distributions agree with this with the exception of horizon #14 which most likely has a higher average velocity and similar velocity values.

Velocity distributions are more closely examined by looking at velocities for horizon #13 (Figure 21). As the population of krill increases over time the more erratic (and higher) the velocity values. It can be concluded that the tracking method is performing better in lower krill population environments, calculating more accurate along-track velocities, than in high population environments.

Velocity Distribution Statistics

Horizon	Total # of velocities	V_{ave}(m/s)	% outlier V
6	603	1.8	22.4%
7	88	1.3	14.8%
12	976	1.9	17.9%
13	2,475	1.6	11.5%
14	6,785	2.5	7.29%

Table 5: The number of velocities (m/s) tracked, average values and percentage of outlier velocities (Figure 20b) are tabled for dive 15. Horizon #14 had the greatest number of velocities tracked but the lowest percentage of outliers.

1.4 Discussion

Tracking and quantifying krill motion data *in situ* in the open water column is an evolving problem that is not without error. Reconstructing tracks in three dimensions using stereo geometry and triangulation methods revealed that poor depth estimates in the camera relative z-direction and produces errors when calculating krill positions and velocities in three dimensions (Figure 14 and 19). Error in z is most likely from two sources: triangulation and bad stereo matching. Depth

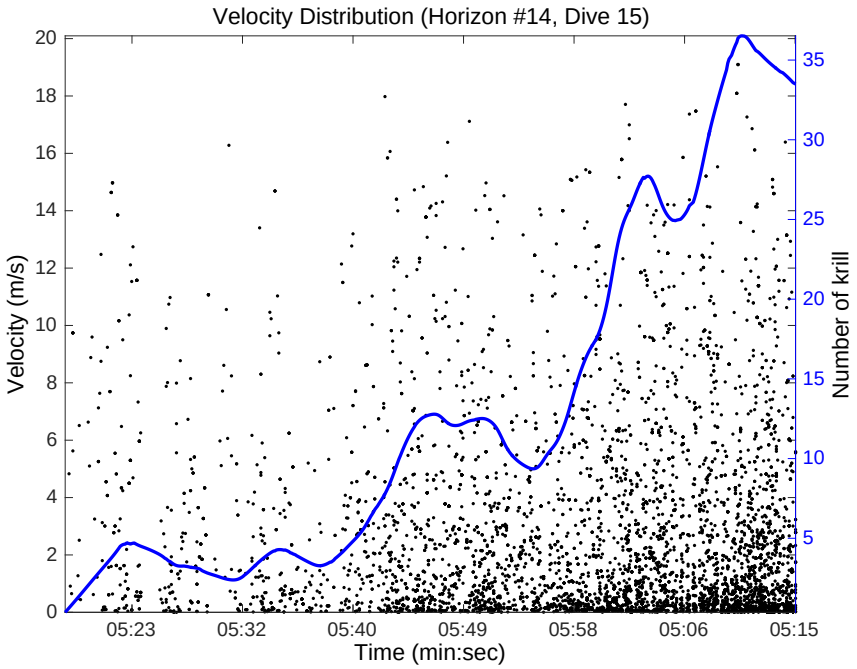

Figure 21: The number of observed velocities increases over time during horizon#14, dive 15.

estimation is very sensitive to changes in the pixel position of the matched krill. If the centroids are not initially identified correctly (during segmentation) the point matching between the left and right images will provide a poor stereo triangulation [1, 28]. Alternatively if a krill was matched incorrectly in the adjacent image, it's position estimate in three dimensional space will be wrong. This weakness in triangulation and depth position estimation contributed to most of the velocity error.

The automated tracking algorithm successfully tracks 60% to 80% of krill in an image (Table 4 and Figure 17) using a discrete, two-step tracking method (Figure 10). A traditional linear model-based approach, such as a Kalman Filter, was not used as krill motion is generally non-linear [32]. Krill do not exhibit linear, predictable trajectories when swarming, stalling or rapidly accelerating that can

be reliably modeled [3, 20, 10, 11, 2]. The automated tracking method strives to account for these krill behaviors by estimating position based on the prior krill motion vectors along-track and considering all possible matches within an empirically determined search radius of the estimated new position (Figure 14).

More robust depth triangulation would aid in tracking krill in three dimensions. This would also improve the krill velocity calculations (Figures 14 and 19, Tables 2 and 3), and existing observed and modeled krill velocities used in behavioral studies [11, 3, 20, 2, 7, 12, 25, 13, 19]. Other improvements to the matching include creating a variable-sized krill template that conforms to the size of each krill when solving the SSD and adding range constraints to increase the robustness of the SSD [1, 23, 28]. Also a higher camera sampling rate than the current $10Hz$ should be considered in instances of high krill populations. Better tracking in dense aggregations would increase the amount of available krill behavioral data in swarms that potentially impact surrounding physical ocean processes [3, 9, 33].

Additionally, krill velocity ensemble statistics further confirm that the tracking method more accurately observes krill in low-population environments (Figures 20 and 21). Velocities observed in lower population images corroborate earlier work [10, 30, 31]. The tracking method can now be used to generate large motion data sets to further study behavioral patterns of krill. In turn, these can better inform Antarctic circulation study parameters since the WAP is one of the most affected regions by seasonal sea ice flows which provides a crucial habitat and survival mechanism for krill larve and juvenile communities as discussed in [34, 35, 8, 30]. Ecosystem management and conservation policies would also greatly benefit from a better understanding of krill behavior in the Southern Ocean as described in [5].

The image data collected by the camera sled instrumentation system combines traditional sampling methods (CTD and ADCP) with stereo camera image

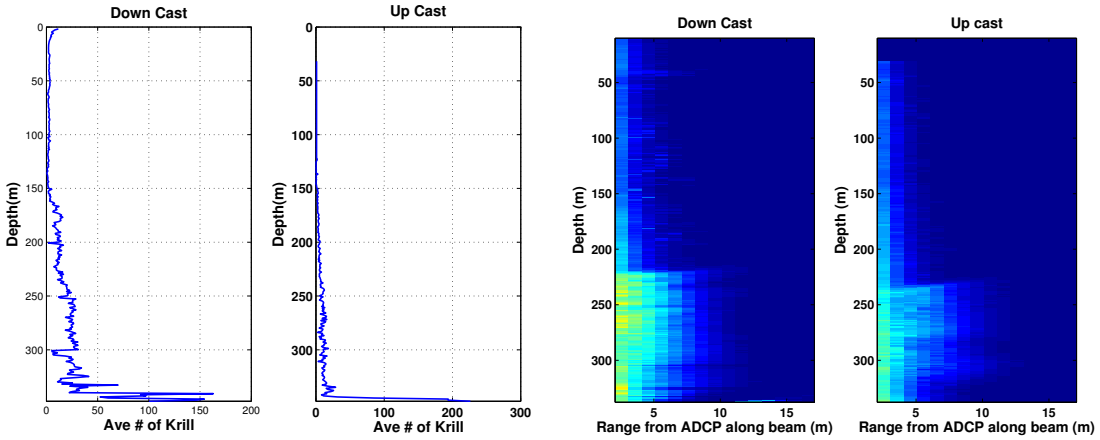

(a) (b)

Figure 22: A comparison of average krill abundances for dive 15. (a) Krill abundances from the image data are compared to (b) ADCP backscatter intensities. Both show similar abundance trends for dive 15 (May 25, 2013 in Andvord Bay).

data. This combination has the potential to compare krill track data directly to acoustic krill data (Figure 22) [36, 21, 2, 25, 37]. It improves upon the currently available imaging systems (both *in situ* and in the lab environment) and generates quantitative physical and behavioral zooplankton data [3, 10, 13, 38, 39, 14, 27]. The camera sled system can be deployed for future studies of Antarctic krill or other zooplankton species.

1.5 Conclusions

In conclusion, the automated krill tracking algorithm can track krill *in situ* in both two dimensional camera relative units and in three dimensions using stereo reconstruction. The automated tracking algorithm and track library are tools that provide detailed access to the behavior of individual animals. *In situ* track data helps refine and expand the available methods to study krill motion and behavioral patterns.

LIST OF REFERENCES

[1] R. Hartley and A. Zisserman, *Multiple view geometry in computer vision*. Cambridge university press, 2003.

[2] S. Nicol and A. Brierley, "Through a glass less darkly - new approaches for studying the distribution, abundance and biology of euphausiids," *Deep-Sea Research II*, vol. 57, pp. 496–507, 2010.

[3] W. Hamner and P. Hamner, "Behavior of antarctic krill (*euphasia superba*): schooling, foraging, and antipredatory behavior," *Canadian Journal of Fisheries and Aquatic Sciences*, vol. 57, no. 3, pp. 192–202, 2000.

[4] A. S. Brierley, "Antarctic ecosystem: Are deep krill ecological outliers or portents of a paradigm shift?" *Current Biology*, vol. 18, no. 6, pp. R252 – R254, 2008. [Online]. Available: http://www.sciencedirect.com/science/article/pii/S0960982208000687

[5] J. A. Nilsson, E. A. Fulton, M. Haward, and C. Johnson, "Consensus management in antarctica's high seas past success and current challenges," *Marine Policy*, vol. 73, pp. 172 – 180, 2016.

[6] K. Banse, "Zooplankton: Pivotal role in the control of ocean production i. biomass and production," *ICES Journal of Marine Science: Journal du Conseil*, vol. 52, no. 3-4, pp. 265–277, 1995.

[7] S. Nicol, "Krill, currents, and sea ice: Euphausia superba and its changing environment," *BioScience*, vol. 56, no. 2, pp. 111–120, 2006.

[8] S. Thorpe, E. Murphy, and J. Watkins, "Circumpolar connections between antarctic krill (euphausia superba dana) populations: investigating the roles of ocean and sea ice transport," *Deep Sea Research I*, vol. 54, no. 5, pp. 792–810, February 2007.

[9] P. Wiebe, C. Ashjian, G. Lawson, A. Piñones, and N. Copley, "Horizontal and vertical distribution of euphausiid species on the western antarctic peninsula u.s. globec southern ocean study site," *Deep Sea Research II*, vol. 58, pp. 1630–1651, 2011.

[10] S. W. Strand and W. M. Hamner, "Schooling behavior of antarctic krill (euphausia superba) in laboratory aquaria: Reactions to chemical and visual stimuli," *Marine Biology*, vol. 106, no. 3, pp. 355–359, 1990. [Online]. Available: http://dx.doi.org/10.1007/BF01344312

[11] M. K. Kane, "Winter vertical distributions of antarctic krill as seen through a new stereo camera system," Master's thesis, Graduate School of Oceanography - University of Rhode Island, 2015.

[12] T. Letessier, S. Kawaguchi, R. King, J. Meeuwig, R. Harcourt, and M. Cox, "A robust and economical underwater stereo video system to observe antarctic krill (euphausia superba)," *Open Journal of Marine Science*, vol. 3, no. 3, pp. 148–153, 2013.

[13] C. J. Ashjian, C. S. Davis, S. M. Gallager, P. H. Wiebe, and G. L. Lawson, "Distribution of larval krill and zooplankton in association with hydrography in marguerite bay, antarctic peninsula, in austral fall and winter 2001 described using the video plankton recorder," *Deep Sea Research Part II: Topical Studies in Oceanography*, vol. 55, no. 34, pp. 455 – 471, 2008, dynamics of Plankton, Krill, and Predators in Relation to Environmental Features of the Western Antarctic Peninsula and Related Areas: {SO} {GLOBEC} Part {II}. [Online]. Available: http://www.sciencedirect.com/science/article/pii/S096706450700313X

[14] K. D. Mankoff and T. A. Russo, "The kinect: a low-cost, high-resolution, short-range 3d camera," *Earth Surface Processes and Landforms*, vol. 38, no. 9, pp. 926–936, 2013. [Online]. Available: http://dx.doi.org/10.1002/esp.3332

[15] C. J. Ashjian, C. S. Davis, S. M. Gallager, and P. Alatalo, "Distribution of plankton, particles, and hydrographic features across georges bank described using the video plankton recorder," *Deep Sea Research Part II: Topical Studies in Oceanography*, vol. 48, no. 13, pp. 245 – 282, 2001, coupled biological and physical studies of plankton populations on Georges Bank and related North Atlantic regions. [Online]. Available: http://www.sciencedirect.com/science/article/pii/S0967064500001211

[16] M. Benfield, S. Cabell, P. Wiebe, S. Gallager, R. Lough, and N. Copley, "Video plankton recorder estimates of copepod, pteropod and larvacean distributions from a stratified region of georges bank with comparative measurements from a mocness sampler," *Deep Sea Research II*, vol. 43, no. 7–8, pp. 1925–1945, 1996.

[17] E. Broughton and R. Lough, "A direct comparison of mocness and video plankton recorder zooplankton abundance estimates: Possible applications for augmenting net sampling with video systems," *Deep Sea Research II*, vol. 53, pp. 2789–2807, 2006.

[18] P. Wiebe, S. Boyd, B. Davis, and J. Cox, "Avoidance of towed nets by the euphausiid *nematoscelis megalops*," *Fishery Bulletin*, vol. 80, no. 1, pp. 75–91, 1982.

[19] A. C. Cleary, E. G. Durbin, M. C. Casas, and M. Zhou, "Winter distribution and size structure of antarctic krill euphausia superba populations in-shore along the west antarctic peninsula," *Marine Ecology Progress Series*, vol. 552, pp. 115–129, 2016.

[20] L. Quentin and R. Ross, "Behavioral and physiological characteristics of the antarctic krill, euphasia superba," *American Zoologist*, vol. 31, no. 1, pp. 49–63, 1991.

[21] G. Lawson, P. Wiebe, C. Ashjian, D. Chu, and T. Stanton, "Improved parameterization of antarctic krill target strength models," *Journal of the Acoustical Society of America*, vol. 119, no. 1, pp. 232–242, 2006.

[22] R. C. Gonzalez and R. E. Woods, *Digital Image Processing*, 3rd ed. Pearson Education Inc., 2008, ch. 9-10.

[23] J. D. Gibson and A. Bovik, Eds., *Handbook of Image and Video Processing*, 1st ed. Orlando, FL, USA: Academic Press, Inc., 2000, ch. 3.12.

[24] N. Otsu, "A threshold selection method from gray-level histograms," *IEEE Transactions on Systems, Man and Cybernetics*, vol. 9, no. 1, pp. 62–66, 1979.

[25] M. J. Cox, J. D. Warren, D. A. Demer, G. R. Cutter, and A. S. Brierley, "Three-dimensional observations of swarms of antarctic krill (euphausia superba) made using a multi-beam echosounder," *Deep Sea Research Part II: Topical Studies in Oceanography*, vol. 57, no. 78, pp. 508 – 518, 2010, krill Biology and Ecology: Dedicated to Edward Brinton 1924-2010.

[26] E. Kreyszig, *Advanced Engineering Mathematics*, 10th ed. John Wiley & Sons Inc., 2011, ch. 9.

[27] J. Rife and S. M. Rock, "Segmentation methods for visual tracking of deep-ocean jellyfish using a conventional camera," *Oceanic Engineering, IEEE Journal of*, vol. 28, no. 4, pp. 595–608, Oct. 2003.

[28] B. K. Horn, "Relative orientation," *International Journal of Computer Vision*, vol. 4, no. 1, pp. 59–78, 1990.

[29] J.-Y. Bouguet, "Camera Calibration Toolbox for Matlab," retrieved July 2014.

[30] G. A. Tarling and S. E. Thorpe, "Instantaneous movement of krill swarms in the antarctic circumpolar current," *Limnology and Oceanography*, vol. 59, no. 3, pp. 872–886, 2014.

[31] W. M. Hamner, "Aspects of schooling euphasia superba," *Journal of Crustacean Biology*, vol. 4, no. 5, pp. 67–74, 1984.

[32] S. Thrun, W. Burgard, and D. Fox, *Probabilistic Robotics (Intelligent Robotics and Autonomous Agents)*. The MIT Press, 2005, ch. 2-3.

[33] A. Renner, S. Thorpe, K. Heywood, E. Murphy, J. Watkins, and M. Meredith, "Advective pathways near the tip of the antarctic peninsula: Trends, variability and ecosystem implications," *Deep-Sea Research I*, vol. 63, pp. 91–101, 2012.

[34] B. A. Fach and J. M. Klinck, "Transport of antarctic krill (euphausia superba) across the scotia sea. part i: Circulation and particle tracking simulations," *Deep Sea Research Part I: Oceanographic Research Papers*, vol. 53, no. 6, pp. 987 – 1010, 2006.

[35] B. A. Fach, E. E. Hofmann, and E. J. Murphy, "Transport of antarctic krill (euphausia superba) across the scotia sea. part ii: Krill growth and survival," *Deep Sea Research Part I: Oceanographic Research Papers*, vol. 53, no. 6, pp. 1011–1043, 2006.

[36] C. Greene, T. Stanton, P. Wiebe, and S. McClatchie, "Letter to nature," January 1991.

[37] M. Zhou and R. D. Dorland, "Aggregation and vertical migration behavior of euphausia superba," *Deep Sea Research Part II: Topical Studies in Oceanography*, vol. 51, no. 1719, pp. 2119 – 2137, 2004, integrated Ecosystem Studies of Western Antarctic Peninsula Continental Shelf Waters and Related Southern Ocean Regions. [Online]. Available: http://www.sciencedirect.com/science/article/pii/S0967064504001262

[38] S. Menden-deuer and D. Grnbaum, "Individual foraging behaviors and population distributions of a planktonic predator aggregating to phytoplankton thin layers," *Limnol. Oceanogr*, pp. 109–116, 2006.

[39] E. L. Harvey and S. Menden-Deuer, "Avoidance, movement, and mortality: The interactions between a protistan grazer and heterosigma akashiwo, a harmful algal bloom species," *Limnology and Oceanography*, vol. 56, no. 1, pp. 371–378, 2011. [Online]. Available: http://dx.doi.org/10.4319/lo.2011.56.1.0371

APPENDIX A

Larger Map of Sampling Area

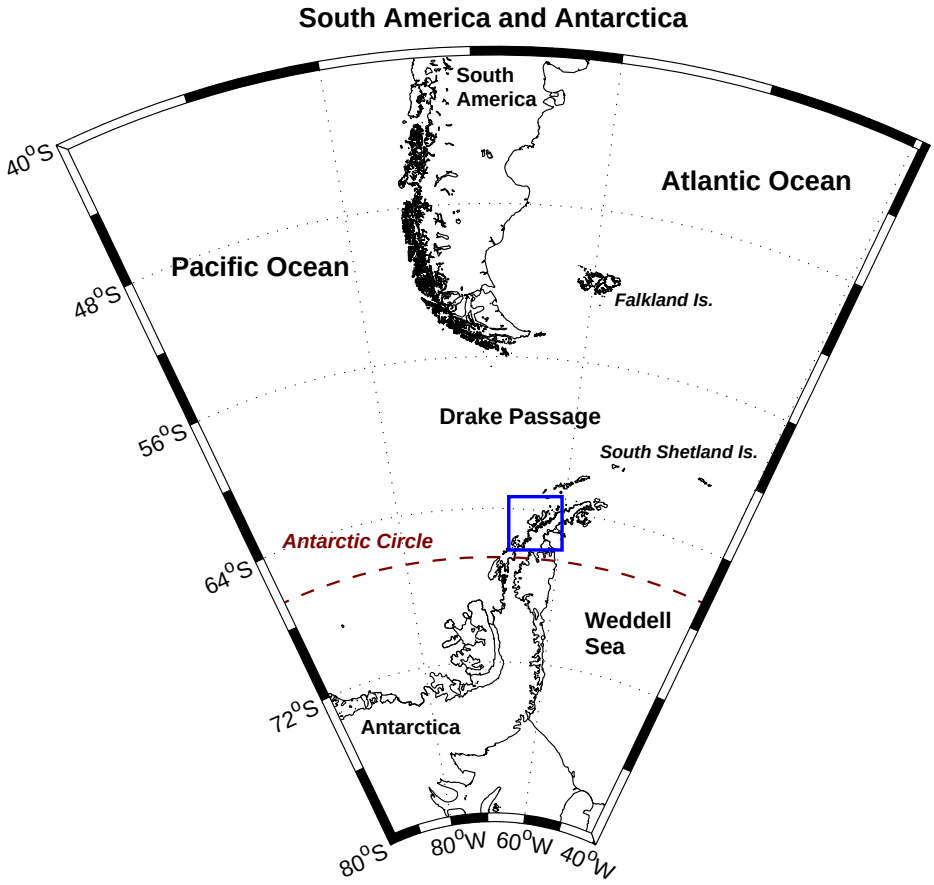

Figure A.1: The Western Antarctic Peninsula (WAP) relative to southern tip of Southern America. The blue box denotes the camera sled deployment area during the 2013 austral winter.

APPENDIX B

Stereo Rectification and Epipolar Geometry

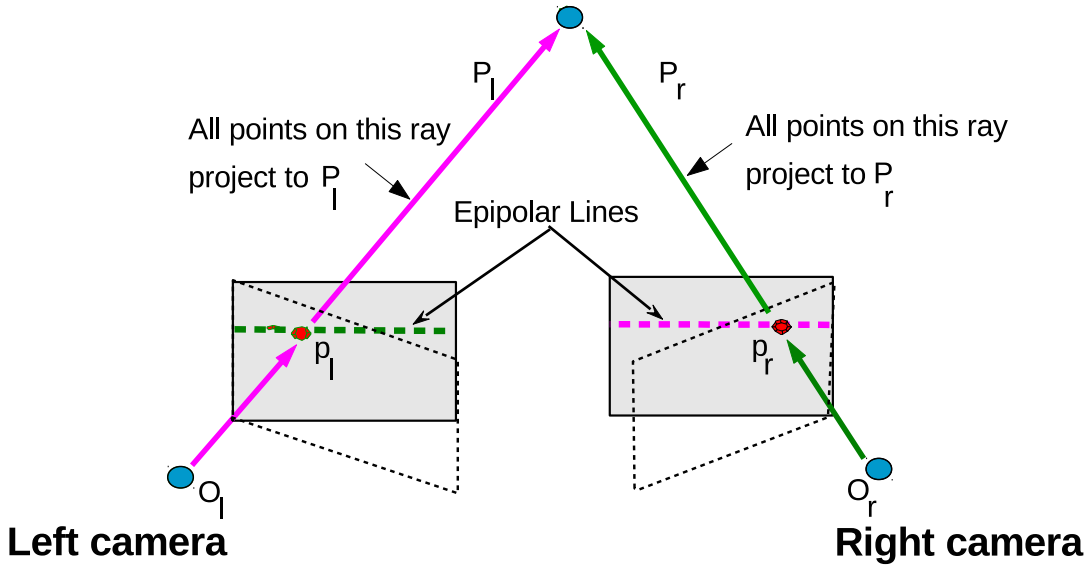

Figure B.1: An example of how two images are made coplanar during stereo rectification. A projective transform is applied to one image (using epipolar geometry) to align with the second image [1].

APPENDIX C

The Elliptical Structuring Element

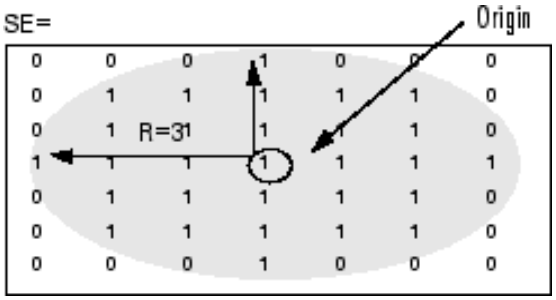

Figure C.1: An elliptical structuring element with a radius of three. (Image courtesy of: https://www.mathworks.com)

The elliptical shape (Figure C.1) was chosen for the following reasons.

- Ellipses are rotationally invariant.
- Prior camera configuration (calibration and focus) helped estimate the ellipse size needed to identify krill.
- A structuring element collates region properties (area, major and minor axes) for each identified krill (step # 4) [22, 23].

APPENDIX D

Krill Tracking: decision tree

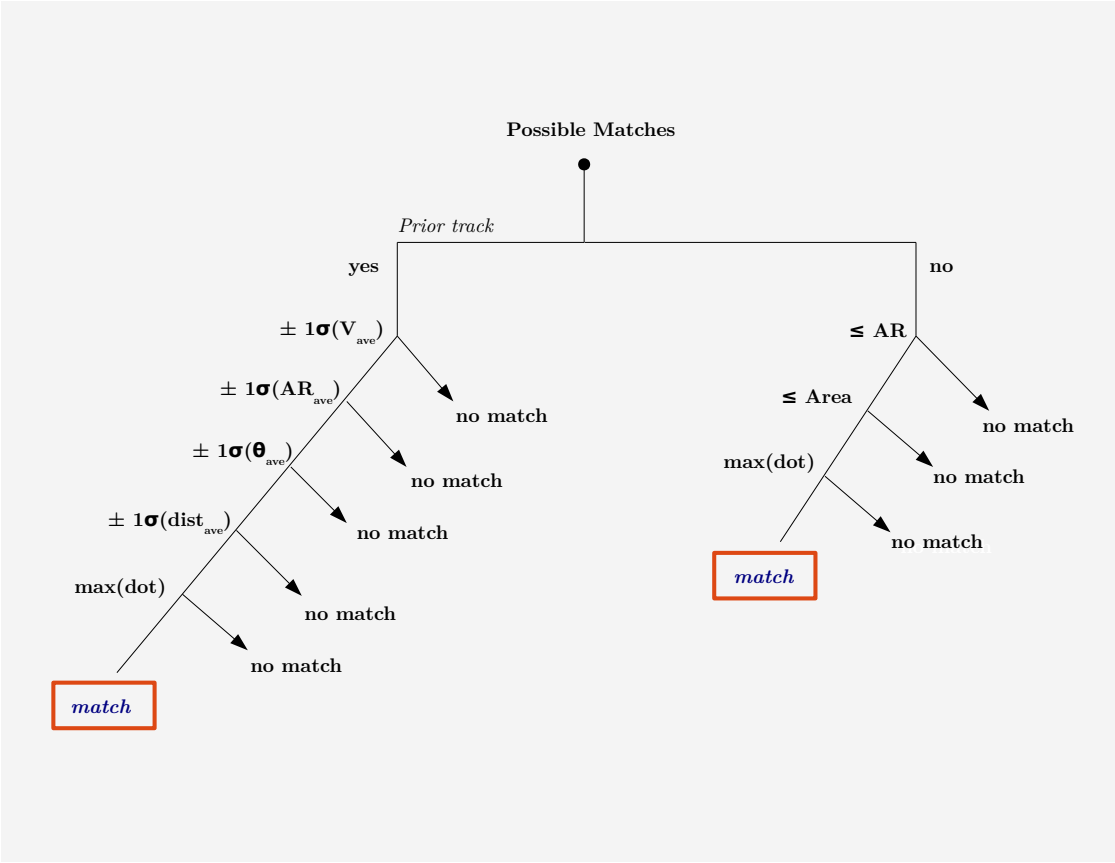

Figure D.1: The decision tree that the krill tracking method uses to determine matches between image frames. If a krill has a prior track, the average and standard deviations for several recorded variables are used to choose the matching krill.